Group refractive index and group velocity dispersion measurement by complex master slave interferometry

SYLVAIN RIVET,[1,*] ADRIAN BRADU,[2] FIONA BAIRSTOW,[2] HISHAM FORRIÈRE,[2] AND ADRIAN PODOLEANU[2]

[1]*Laboratoire d'Optique et de Magnétisme EA 938, Université de Bretagne Occidentale, IBSAM, 6 avenue Le Gorgeu, C.S. 93837, 29238 Brest Cedex 3, France*
[2]*Applied Optics Group, School of Physical Sciences, University of Kent, Canterbury CT2 7NH, UK*
**sylvain.rivet@univ-brest.fr*

Abstract: This paper demonstrates that the complex master slave interferometry (*CMSI*) method used in spectral domain interferometry (*SDI*) can efficiently be used for accurate refractive index and group velocity dispersion measurements of optically transparent samples. For the first time, we demonstrate the relevance of the phase information delivered by *CMSI* for dispersion evaluations with no need to linearize data. The technique proposed here has been used to accurately measure the group refractive index and the group velocity dispersion of a strong dispersive sample (SF6 glass), and a weak dispersive one (distilled water). The robustness of the technique is demonstrated through the manipulation of several sets of experimental data.

OCIS codes: (120.0120) Instrumentation, measurement, and metrology; (110.4500) Optical coherence tomography.

References and links

1. J. G. Fujimoto, "Optical coherence tomography for ultrahigh resolution in vivo imaging," Nat. Biotechnol. **21**(11), 1361–1367 (2003).
2. D. Huang, E. A. Swanson, C. P. Lin, J. S. Schuman, W. G. Stinson, W. Chang, M. R. Hee, T. Flotte, K. Gregory, C. A. Puliafito, and J. G. Fujimoto, "Optical coherence tomography," Science **254**(5035), 1178–1181 (1991).
3. W. V. Sorin and D. F. Gray, "Simultaneous thickness and group index measurement using optical low-coherence reflectometry," IEEE Photonics Technol. Lett. **4**(1), 105–107 (1992).
4. J. Na, H. Y. Choi, E. S. Choi, C. Lee, and B. H. Lee, "Self-referenced spectral interferometry for simultaneous measurements of thickness and refractive index," Appl. Opt. **48**(13), 2461–2467 (2009).
5. P. Hlubina, "White-light spectral interferometry with the uncompensated Michelson interferometer and the group refractive index dispersion in fused silica," Opt. Commun. **193**(1–6), 1–7 (2001).
6. G. D. Gillen and S. Guha, "Use of Michelson and Fabry-Perot interferometry for independent determination of the refractive index and physical thickness of wafers," Appl. Opt. **44**(3), 344–347 (2005).
7. P. H. Tomlins, P. Woolliams, C. Hart, A. Beaumont, and M. Tedaldi, "Optical coherence refractometry," Opt. Lett. **33**(19), 2272–2274 (2008).
8. S. Kim, J. Na, M. J. Kim, and B. H. Lee, "Simultaneous measurement of refractive index and thickness by combining low-coherence interferometry and confocal optics," Opt. Express **16**(8), 5516–5526 (2008).
9. B. Bräuer, S. G. Murdoch, and F. Vanholsbeeck, "Dispersion measurements in ocular media using a dual-wavelength swept source optical coherence tomography system," Opt. Lett. **41**(24), 5732–5735 (2016).
10. S. C. Zilio, "Simultaneous thickness and group index measurement with a single arm low-coherence interferometer," Opt. Express **22**(22), 27392–27397 (2014).
11. Y. Verma, P. Nandi, K. D. Rao, M. Sharma, and P. Kumar Gupta, "Use of common path phase sensitive spectral domain optical coherence tomography for refractive index measurements," Appl. Opt. **50**(25), E7–E12 (2011).
12. C. Dorrer, "Influence of the calibration of the detector on spectral interferometry," J. Opt. Soc. Am. B **16**(7), 1160–1168 (1999).
13. C. Dorrer, N. Belabas, J.-P. Likforman, and M. Joffre, "Spectral resolution and resampling issues in Fourier-transform spectral interferometry," J. Opt. Soc. Am. B **17**(10), 1795–1802 (2000).
14. A. K. Trull, J. van der Horst, J. G. Bijster, and J. Kalkman, "Transmission optical coherence tomography based measurement of optical material properties," Opt. Express **23**(26), 33550–33563 (2015).
15. N. Lippok, S. Coen, P. Nielsen, and F. Vanholsbeeck, "Dispersion compensation in Fourier domain optical coherence tomography using the fractional Fourier transform," Opt. Express **20**(21), 23398–23413 (2012).

16. K. K. H. Chan and S. Tang, "High-speed spectral domain optical coherence tomography using non-uniform fast Fourier transform," Biomed. Opt. Express **1**(5), 1309–1319 (2010).
17. D. Reolon, M. Jacquot, I. Verrier, G. Brun, and C. Veillas, "High resolution group refractive index measurement by broadband supercontinuum interferometry and wavelet-transform analysis," Opt. Express **14**(26), 12744–12750 (2006).
18. A. G. Podoleanu and A. Bradu, "Master-slave interferometry for parallel spectral domain interferometry sensing and versatile 3D optical coherence tomography," Opt. Express **21**(16), 19324–19338 (2013).
19. S. Rivet, M. Maria, A. Bradu, T. Feuchter, L. Leick, and A. Podoleanu, "Complex Master Slave Interferometry," Opt. Express **24**(3), 2885–2904 (2016).
20. A. Bradu, S. Rivet, and A. Podoleanu, "Master/Slave interferometry - Ideal tool for coherence revival swept source optical coherence tomography," Biomed. Opt. Express **7**(7), 2453–2468 (2016).
21. R. Cernat, A. Bradu, N. M. Israelsen, O. Bang, S. Rivet, P. A. Keane, D.-G. Heath, R. Rajendram, A. Podoleanu, "Gabor fusion master slave optical coherence tomography," Biomed. Opt. Lett. **8**(2), 813 (2017).
22. Y. Yasuno, V. D. Madjarova, S. Makita, M. Akiba, A. Morosawa, C. Chong, T. Sakai, K.-P. Chan, M. Itoh, and T. Yatagai, "Three-dimensional and high-speed swept-source optical coherence tomography for in vivo investigation of human anterior eye segments," Opt. Express **13**(26), 10652–10664 (2005).
23. http://www.schott.com
24. M. Daimon and A. Masumura, "Measurement of the refractive index of distilled water from the near-infrared region to the ultraviolet region," Appl. Opt. **46**(18), 3811–3820 (2007).
25. A. Bradu, M. Maria, and A. G. Podoleanu, "Demonstration of tolerance to dispersion of master/slave interferometry," Opt. Express **23**(11), 14148–14161 (2015).
26. C. Photiou, E. Bousi, I. Zouvani, and C. Pitris, "Using speckle to measure tissue dispersion in optical coherence tomography," Biomed. Opt. Express **8**(5), 2528–2535 (2017).
27. T. Kitazawa and T. Nomura, "Refractive index tomography based on optical coherence tomography and tomographic reconstruction algorithm," Jpn. J. Appl. Phys. **56**(9S), 09NB03 (2017).

1. Introduction

Spectral (or Fourier) domain Interferometry (*SDI*) is widely spread in many fields of biomedical optics and sensing. *SDI* is at the core of the modern Optical Coherence Tomography (OCT) [1,2] technology and of group refractive index measurement methods [3]. The measurement of group refractive index of optically transparent samples can be carried out in various ways, very often by using a low-coherence Michelson interferometer [4–9], in which case two measurements are performed: with the sample inserted within one of the interferometer arms and without, or by a single measurement in a common-path interferometer [10,11] for thin samples.

These techniques are based on recovering the spectral phase from the electrical signal at the interferometer output. The electrical signal delivered by the spectrometer is termed in what follows as channeled spectrum, *i.e.* the electrical version of the optical spectrum read by a camera incorporated within a spectrometer. The channeled spectrum is usually chirped due to: (i) the nonlinear dependence of the pixel position in the camera versus the optical frequency and (ii) the unbalanced dispersion between the arms of the interferometer. Before decoding the modulations in the channeled spectrum via a Fourier transform (FT), the chirping has to be canceled out.

Faultless calibration of the spectrometer is crucial, especially when handling a large number of fringes in the spectrum, where calibration errors are amplified. Hence a calibration precision far superior to the instrument optical resolution is required [12]. Indeed, it was shown that calibration accuracy better than one-tenth of the spacing between two consecutive pixels on the camera is often required to achieve the best possible accuracy in the measured spectral phase.

To decode the channeled spectrum and recover the spectral phase, *SDI* uses methods to resample and organize the data linearly along the optical frequency axis from the knowledge of the measured chirp, and apply FTs to the signal. Such decoding algorithms are based on the phase interpolation [13,14] or on more sophisticated data processing methods based on fractional Fourier transform, non-uniform fast Fourier transform and wavelet-transform analysis [15–17].

Master-Slave Interferometry *(MSI)* [18] (and its improved version, Complex Master Slave Interferometry (*CMSI*) [19–21]) represent novel approaches to *SDI*, useful in OCT signal

processing. For the scope of this study, the more efficient algorithm of the CMSI will be employed. This proceeds in two stages. In a first stage (Master), several experimental channeled spectra are acquired by using a mirror as sample. These spectra are affected by the nonlinearity in transducing the optical spectrum into an electrical signal and dispersion in the interferometer, making the electrical output signal chirped. Then, digital local oscillations (named masks in this paper) are generated for as many depths (optical path differences) as required. As the algorithm employs the set of experimentally collected channeled spectra, the masks incorporate the chirp due to nonlinearity in reading the spectra and dispersion in the interferometer. In the second stage (Slave), the sample replaces the mirror. The stored masks are mixed with the channeled spectrum I^{sample} acquired from the sample. It has been demonstrated [21] that, by applying *CMSI*, irrespective of how chirped the I^{sample} signal is, the A-scan profile obtained is identical to that delivered by a Fourier transform of I^{sample} for a perfectly dispersion-compensated interferometer and perfectly linearized decoder (no nonlinear dependence on the pixel position). Thus, there is no need for data resampling and the procedure is free from errors otherwise resulting from the interpolation of the experimental data. Finally, in a previous report [20] we demonstrated that a *CMSI* instrument can produce axial reflectivity profiles faster than the FFT-based conventional methods employing data resampling. This was made possible by harnessing efficient algorithms of manipulating matrices that can be implemented on computer processing units (CPU).

In previous *MSI* [18] and *CMSI* papers [19–21], only amplitude information was employed to produce OCT images without taking advantage of the information incorporated in the phase.

In this paper, we experimentally validate the relevance of phase information that can be delivered by *CMSI*. Thus, we demonstrate that phase information can be used to measure the group refractive index and the group velocity dispersion of optical transparent samples with high accuracy.

2. Phase reconstruction procedure by *CMSI*

In Fig. 1, the schematic diagram of an *SDI* experimental set-up is shown, containing the two main components, an in-fiber interferometer and a spectrometer. The interferometer includes a beam-splitter (shown as a single mode optical fiber directional coupler), a flat reference mirror (M_r), and a flat sample mirror (M_s). The sample to be analyzed is inserted between the sample mirror, M_s, and the achromatic lens L_s. To actuate on the optical path difference (OPD) introduced by the addition of the sample in the sample arm of the interferometer, the mirror M_s is placed on a linear translation stage.

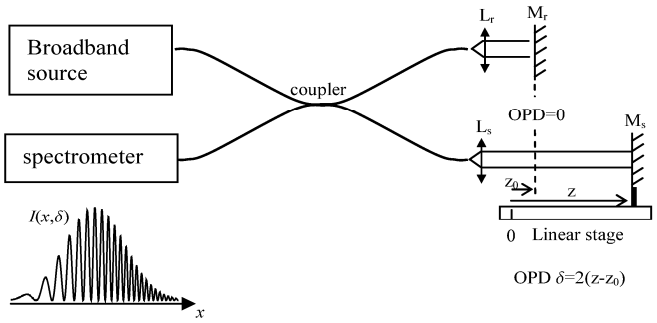

Fig. 1. Block diagram of a spectral domain interferometer. M_r and M_s are respectively the reference mirror and the sample mirror. The mirror M_s can be moved along the optical axis by a linear translation stage. The positions z and z_0 correspond to the positions of M_s relatively to the origin 0 of the linear stage. $I(x,\delta)$ is the recorded channeled spectrum versus the pixel x of the camera for a given OPD = δ. L_s and L_r are identical achromatic lenses.

The electrical signal at the output of the interferometer shown in Fig. 1 is typically digitized using an image acquisition board (IMAQ) connected to a linear camera via a camera link cable. This electrical signal can be expressed as a function of the pixel position (x) on the spectrometer camera and the OPD = δ in the interferometer by the following equation:

$$I(x,\delta) = I_0\left(p(x)\right)\left(1+\cos\left[\phi\left(p(x),\delta\right)+\phi_0\left(p(x)\right)\right]\right), \quad (1)$$

where $I_0(p(x))$ is the power spectrum of the optical source, $p(x)$ = ω is the relationship between the pixel x and the optical angular frequency ω, $\phi(p(x),\delta) = p(x)\ \delta/c$ is the phase related to δ responsible for the modulation in the spectrum, and ϕ_0 is the additional phase due to the unbalanced dispersion in the interferometer. The OPD can be expressed relatively to the position of the stage where OPD = 0, z_0, and the position of the mirror M_s, z, by $\delta = 2(z-z_0)$.

A widely accepted procedure to extract the phase ϕ from Eq. (1) [22] ignores the additional phase ϕ_0 and proceeds in two sequential steps:

(i) the function $p(x)$ is linearized,

(ii) a Fourier transform is applied to $I(x,\delta)$.

CMSI is equivalent to the steps above but carried out in a single calculation with resulting advantages in terms of procedure simplification and speed. When employing *CMSI*, in a first stage (Master), the sample is replaced with a mirror and several experimental channeled spectra (CS_{exp}) are acquired for different OPD values [19]. These experimental channeled spectra CS_{exp} are chirped due to the non-linearity of the spectrometer, $p(x)$, and due to the unbalanced dispersion described by ϕ_0 according to Eq. (1). The purpose of the Master stage is to measure p and ϕ_0 that are then used to build masks $M(x,t)$, given by:

$$M(x,t) = \frac{dp}{dx} Exp\left[-i\left(\left(p(x)-p(x_c)\right)t+\phi_0\left(p(x)\right)-\phi_0\left(p(x_c)\right)\right)\right]. \quad (2)$$

$M(x,t)$ are then generated digitally versus discrete values of x and t, and stored before being mixed with the channeled spectrum corresponding to the sample. In the equation above, the values for x vary from 1 to the number N of pixels of the camera, x_c is the position of the pixel at the center of the linear camera. The values t are related to the OPD values where *CMSI* calculation returns a reflectivity point of the reflectivity profile in depth, A-scan. They could be any values within the axial range allowed by the interference process. Let us consider a uniformly-spaced range of t values, with an interval equal to the spatial axial resolution limit, $2\pi/\Delta\omega$ where $\Delta\omega$ is the spectral range of the spectrometer equal to the difference $\Delta\omega = p(x_N) - p(x_1)$. For a camera of N pixels, according to Nyquist, only $N/2$ cycles in the channeled spectrum can be sampled. This determines a range of $\pi N/\Delta\omega$ of t values along the OPD coordinate, to accurately represent the A-scan. For such consideration of t values, at least one point is provided for each axial resolution interval.

CMSI consists in calculating a discrete integral between the electrical signal $I(x,\delta)$, converting the channeled spectrum at the output of the interferometer, and the masks, M, as follows:

$$CMSI\left[I(x,\delta)\right] = \sum_{i=1}^{N} I(x_i,\delta)M^*(x_i,t) = FT^{-1}\left[I^{without\ chirp}(\omega,\delta)\right], \quad (3)$$

where the symbol * signifies complex conjugate. The result is equivalent to the inverse Fourier transformation (FT^{-1}) of the complex signal created by reading the channeled spectra $I^{without\ chirp}$ [17] expressed according to:

$$I^{without\ chirp}(\omega,\delta) = I_0(\omega)\,Exp\left[i\,\phi(\omega,\delta)\right]. \quad (4)$$

The ultimate quantity to be obtained is the phase of the signal $I(x,\delta)$. Using *CMSI* there is no need to resample the channeled spectra nor remove the uncompensated chirp because the channeled spectra are expressed as a combination of local oscillators (masks) according to δ, spectra that already contain the chirp measured at the Master stage. Thus, by calculating the Fourier transform and the argument of *CMSI*[*I*], it is possible to extract the phase $\phi(\omega,\delta)$ in Eq. (4) equal to:

$$\phi(\omega,\delta) = Arg\left[FT\left[CMSI\left[I(x,\delta)\right]\right]\right]. \quad (5)$$

Equation (5) describes the phase of the signal at the output of a perfect interferometer (calibrated and perfectly balanced for dispersion), when the OPD between its arms is δ. In such a perfect interferometer, when a sample is placed in one of the arms of the interferometer, for the same δ, the alteration of the phase is exclusively due to the dispersion of that particular sample.

3. Group index and dispersion measurement procedure

Let us consider two channeled spectra $I^{sample}(x,\delta_s)$ and $I^{vacuum}(x,\delta_v)$ recorded respectively with the sample to be investigated placed in the sample arm of the interferometer, and without. The corresponding OPDs δ_s and δ_v can be expressed as $\delta_s = 2(z_s - z_{s0})$, where z_s is the current position of the mirror M_s and z_{s0} is the linear stage position for OPD = 0 with the sample, and $\delta_v = 2(z_v - z_{v0})$, where z_v is the current position of the mirror M_s and z_{v0} is the linear stage position for OPD = 0 without the sample respectively. A set of masks M is built from $M(x,t_0)$ presenting several cycles over N pixels to the densest mask $M(x,t_N)$ whose number of cycles is close to $N/2$ (related to Nyquist frequency). As shown in Fig. 2, $CMSI[I^{vacuum}]$ and $CMSI[I^{sample}]$ are defined with N values in time domain by an interval equal to $2\pi/\Delta\omega$. All values of $CMSI[I^{vacuum}]$ (and $CMSI[I^{sample}]$) are equal to 0 except those corresponding to the product between I^{vacuum} (and I^{sample}) with the set of masks M. The first mask does not start with a zero-cycle in order to remove the DC component of the channeled spectra

The instantaneous phases ϕ^{sample} and ϕ^{vacuum} related to I^{sample} and I^{vacuum} can be measured according to the procedure described in Section 2 and explained in Fig. 2.

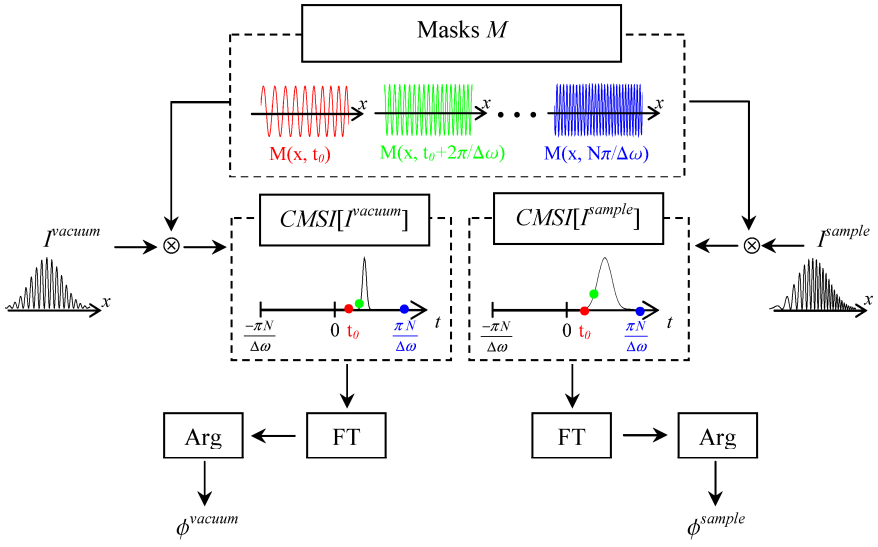

Fig. 2. Block diagram showing the procedure of extracting the spectral phases ϕ^{vacuum} and ϕ^{sample} from the channeled spectra I^{vacuum} and I^{sample} respectively. Masks M, $CMSI[I^{vacuum}]$ and $CMSI[I^{sample}]$ are complex quantities, only their amplitudes are represented in this diagram.

Due to the properties of *CMSI*, the instantaneous phases, free from the non-linearity of the spectrometer and the unbalanced dispersion of the interferometer without sample, can be written as:

$$\phi^{vacuum}(\omega,\delta)=\frac{\omega}{c}\delta_v=\frac{\omega}{c}2(z_v-z_{0v}), \tag{6}$$

$$\phi^{sample}(\omega,\delta)=\frac{\omega}{c}\delta_s=\frac{\omega}{c}2(z_s-z_{0s}), \tag{7}$$

where $z_{0s} = z_{0v}$-(n(ω)-1)e due to the addition of the sample whose thickness is e and refractive index is n(ω).

The phase difference $\Delta\phi = \phi^{sample} - \phi^{vacuum}$ can then be expressed as:

$$\Delta\phi(\omega)=2\frac{\omega}{c}\left[z_s-z_v+(n(\omega)-1)e\right]. \tag{8}$$

The dependence Δϕ vs ω can be fitted by a quadratic form:

$$\Delta\phi(\omega)=\alpha+\beta(\omega-\omega_c)+\gamma(\omega-\omega_c)^2, \tag{9}$$

where ω_c is the angular frequency at the center of the spectrometer given by the function p measured during the Master stage (*i.e.,* $\omega_c = p(x_c)$). The coefficients β and γ are defined according to the derivatives of Δϕ with respect to ω, as:

$$\beta=\left.\frac{d\Delta\phi}{d\omega}\right|_{\omega_c}=\frac{2}{c}(z_s-z_v-e)+\frac{2}{c}e\,n_g(\omega_c), \tag{10}$$

$$\gamma=\frac{1}{2}\left.\frac{d^2\Delta\phi}{d\omega^2}\right|_{\omega_c}=GDD(\omega_c), \tag{11}$$

where the group refractive index $n_g(\omega_c)$ is defined by the derivative d(ω n)/dω, whilst the group delay dispersion *GDD* at an angular frequency ω_c is defined by $e\,c^{-1}$ d^2(ω n)/dω^2.

Thus, if the thickness e is known, the group index and the group velocity dispersion (*GVD*) can be recovered employing respectively the linear and quadratic coefficients in Eq. (9) as:

$$n_g(\omega_c)=\frac{c\beta/2+z_v-z_s}{e}+1, \tag{12}$$

$$GVD(\omega_c)=\frac{GDD(\omega_c)}{e}=\frac{\gamma}{e}. \tag{13}$$

In practice, to avoid any possible phase wrapping, Δϕ is calculated directly from the following equation:

$$\Delta\phi=Arg\left[FT\left[CMSI\left[I^{sample}(x,\delta_s)\right]\right]\times FT\left[CMSI\left[I^{vacuum}(x,\delta_v)\right]\right]^*\right]. \tag{14}$$

4. Experimental results

The spectrometer has been designed to measure a spectral range of 70 nm with a resolution of 0.068 nm. The camera used in the spectrometer is the line scan camera AViiVA M2 CL with 1024 pixels that operates at its maximum speed (28 kHz). As a light source, a super luminescent diode (SLD, Superlum, Cork, Ireland, model Broadlighter 890) with an 890 nm

central wavelength and a 150 nm spectral bandwidth is employed. This light source uses a combination of 4 SLD modules. In this paper only the two shorter wavelength SLDs are switched on, *i.e.* two SLDs centered at 860 nm and 890 nm covering 70 nm of the spectrometer. The normalized spectrum of the two SLDs emitted by this particular source is shown in Fig. 3(a). The optical power is 0.4 mW in the sample arm and 0.65 mW in the reference arm. Sensitivity is 90 dB close to zero optical path difference, with a drop of 30 dB over 2 mm, which is typical for a spectrometer-based OCT system.

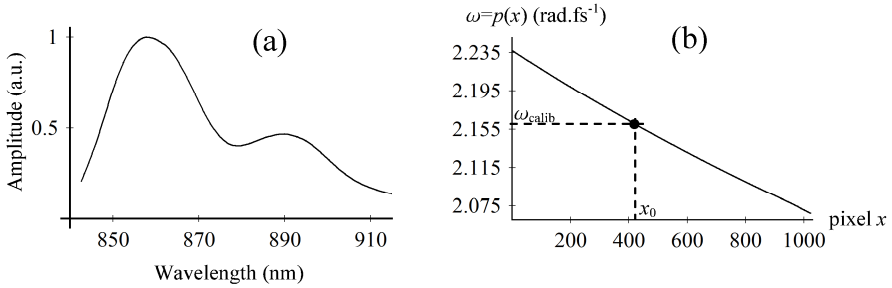

Fig. 3. (a) SLD spectrum as seen by the linear camera. (b) Dependence of the optical angular frequency $\omega = p(x)$ versus pixel position on the camera x. The pixel x_0 corresponds to the incident position of light from a 0.873 mm-line of the swept-source used for calibration.

Because the function p measured during the Master stage is known up to an additive constant, the spectrometer is calibrated with a swept source covering a spectral range from 828 to 873 nm with a wavelength adjustment step of 0.05 nm (line-width equal to 0.045 nm). The 0.873 mm-line of the swept-source, corresponding to an angular frequency $\omega_{calib} = 2.159$ rad.fs^{-1}, has been used for the calibration. This has illuminated the 427th pixel x_0 of the CCD line camera of the spectrometer (Fig. 3(b)).

In order to demonstrate that the proposed method can be used to accurately measure the group refractive index and a large range of group delay dispersion values, two types of materials were considered, with strong and weak dispersion. Two slabs from such materials were sequentially placed in one of the interferometer's arms and their dispersion evaluated using our approach.

4.1 SF6 glass sample

The glass sample SF6 is a 20 mm-flint glass whose catalogue data gives a group index n_g = 1.8205 and group velocity dispersion GVD = 173.37 fs^2/mm at the central pixel of the camera $\omega_c = 2.145$ rad.fs^{-1}, *i.e.* $\lambda_c = 0.8788$ mm [23].

The channeled spectrum I^{vacuum} (Fig. 4(a)) is recorded without the glass being placed in the sample arm of the interferometer for the position of the mirror M_s, z_v = 20.1 mm. When the glass is placed in the sample arm, the mirror M_s is adjusted so that the main spectral modulation of the channeled spectrum I^{sample} (Fig. 4(c)) is similar to that of I^{vacuum} (z_s = 3.695 mm). I^{vacuum} and I^{sample} are recorded 10 times in order to assess the accuracy of n_g and GVD measurements given in the form of (mean +/– 2 standard deviation). The standard deviations for n_g and GVD are related to random noise coming from data-acquisition noise.

The difference between the instantaneous phases $\Delta\phi$ of the two spectra is calculated by applying *CMSI* to I^{sample} and I^{vacuum} (Fig. 4(b) and 4(d)) and using Eq. (14). Because fringe visibility is very weak at the edge of the spectra, $\Delta\phi$ - $\Delta\phi(\omega_c)$ is not plotted over the all spectrum range (Fig. 4(e)). A fit by a quadratic polynomial centered at ω_c, leads to n_g = 1.8203 +/– 0.0001 and GVD = (173 +/– 2) fs^2/mm. The experimental results are in good agreement with the theoretical values. There is a consistent deviation between the experimental and theoretical values of n_g. Its consistency and the fact that the difference is larger than the standard deviation suggest a deterministic bias and not randomness. This

deviation can be explained by the accuracy in measuring the thickness of the sample. For instance, if a 19.995 mm-sample was considered, then we would obtain a perfect match with the theoretical value for n_g.

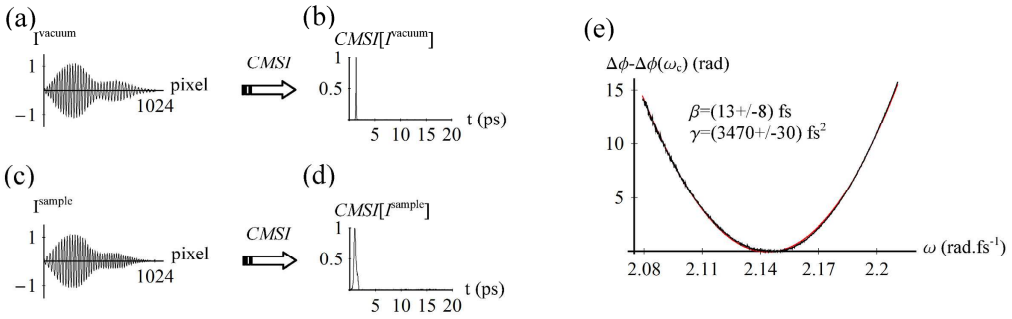

Fig. 4. (a) Channeled spectrum I^{vacuum} without sample in the arm of the interferometer, after filtering the DC component. (b) Calculation of $CMSI[I^{vacuum}]$, where its amplitude is shown only for t>0. (c) Channeled spectrum I^{sample} with sample placed in the sample arm of the interferometer and after filtering the DC component. (d) Calculation of $CMSI[I^{sample}]$, where its amplitude is shown only for t>0. (e) From Eq. (14), $\Delta\phi$-$\Delta\phi(\omega_c)$ is displayed in black curve between 2.08 and 2.2 rad.fs^{-1}. The red curve corresponds to the fit of $\Delta\phi$-$\Delta\phi(\omega_c)$ using as numerical values for the constants in Eq. (9) the values shown in the inset.

These results have been obtained using channeled spectra measured for specific positions of M_s. In order to evaluate the dependence of method accuracy on positions z_v and z_s, *GVD* and n_g have been computed for different sets of channeled spectra. Thus, channeled spectra were recorded, without the sample in place from z_v = 20 mm to 20.4 mm in steps of 50 mm, and with the SF6 glass inserted, from z_s = 3.545 mm to 3.945 mm in steps of 50 mm. Figure 5(a) shows the relative error of *GVD* according to the position of M_s, given by a line corresponding to β = 0. Indeed the specific set (z_v = 20.1 mm, z_s = 3.695 mm), described above and represented by a white circle in Fig. 5(a), has a very weak linear coefficient β (Fig. 4(e)), while the sets of positions from either side of the line (z_v = 20.1 mm, z_s = 3.645 mm) and (z_v = 20.1 mm, z_s = 3.745 mm) have a linear coefficient β different from 0 as shown in Fig. 5(b) and Fig. 5(c). The fact that β = 0 means that the OPD δ_s is equal to δ_v according to the shift theorem of Fourier transform, *i.e.* the main spectral modulation of I^{sample} is identical to that obtained for I^{vacuum}. This condition is more general than the comparison between the position of the peaks in Fourier domain because it is related to the barycenter of the peaks under energy and it is independent from their shape.

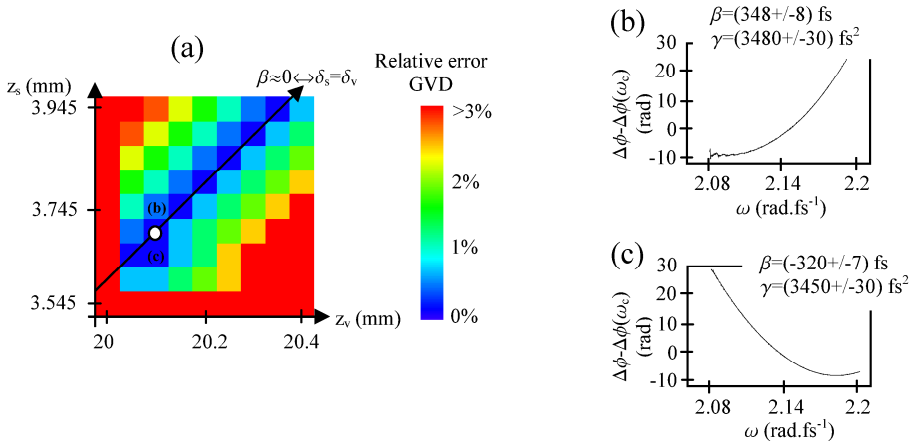

Fig. 5. (a) Relative error of *GVD* according to the position of the mirror M_s with and without the sample in the interferometer's arm. The white circle corresponds to the specific configuration z_v = 20.1 mm and z_s = 3.695 mm used at the beginning of Section 4.1. (b) $\Delta\phi$-$\Delta\phi(\omega_c)$ for the configuration z_v = 20.1 mm and z_s = 3.745 mm. (c) $\Delta\phi$-$\Delta\phi(\omega_c)$ for the configuration z_v = 20.1 mm and z_s = 3.645 mm.

To assess the stability of the measurement, *GVD* has been evaluated along the line corresponding to $\delta_s = \delta_v$ in Fig. 5(a). Figure 6 shows the results, exhibiting a constant *GVD* value, which proves the robustness of the *CMSI* method. *GVD* is not displayed for OPDs inferior to 300 mm because the small number of modulations does not permit to completely separate the DC peak from the peak associated to the modulation, which leads to a greater inaccuracy. Moreover, the study has been carried out until an OPD equal to 1 mm. Indeed *GVD* should be affected by the loss of fringe visibility for high OPDs due to the finite resolution of the spectrometer. The dependence between accuracy and modulation is the same as that applicable to the conventional FT based method because the sensitivity drop off is independent from the specific method used for signal processing, FT or *CMSI*.

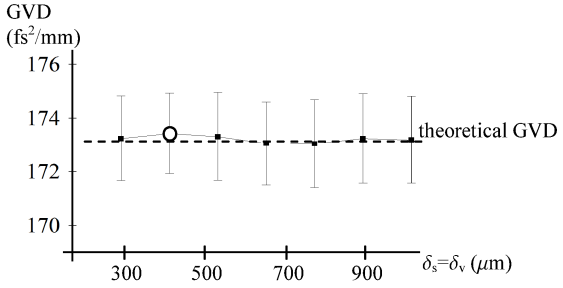

Fig. 6. Measurement of *GVD* for SF6 sample according to the position of the mirror M_s in the case $\delta_s = \delta_v$. The white circle corresponds to the specific configuration z_v = 20.1 mm and z_s = 3.695 mm used in the beginning of Section 4.1.

Figure 7(a) shows the relative error in determining n_g according to the position of M_s. The value n_g is stable irrespective of the position of the mirror M_s except for z_s = 3.545 mm for which the modulation amplitude of the channeled spectrum I^{sample} is not sufficient to perform an accurate measurement. Figure 7(b) exhibits a constant n_g value, which again proves the robustness of the method.

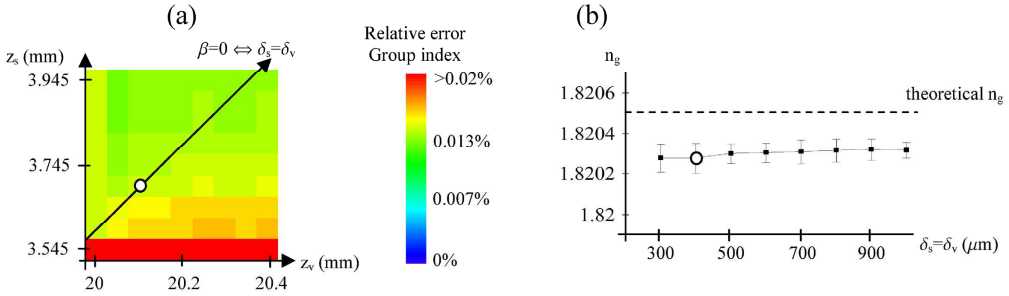

Fig. 7. (a) Relative error of n_g according to the position of the mirror M_s with and without the sample. The white circle corresponds to the specific configuration z_v = 20.1 mm and z_s = 3.695 mm used in the beginning of Section 4.1. (b) Measurement of n_g for SF6 sample according to the position of the mirror M_s in the case $\delta_s = \delta_v$. The thickness of the glass is assumed to be equal to 20 mm for the calculation of n_g.

Note that the loss of fringe visibility due to the finite resolution of the spectrometer has not been taken into account in the current study. In order to measure strong GDD, the loss of fringe visibility should be measured and compensated numerically in order to recover the spectral phase due to the sample only.

4.2 Water sample

Distilled water was used to fill in a rectangular cuvette of 10 mm in length. At the center of the spectrum, *i.e.* λ_c = 0.8788 mm, the theoretical value of the water group index is n_g = 1.3412 and its group velocity dispersion is *GVD* = 16.98 fs^2/mm at 19° C [24].

The Master stage is performed with the empty cuvette in the sample arm so that the dispersion due to the cuvette material itself is taken into account. Avoiding the measurement or compensation procedures for the cuvette dispersion is a practical advantage for *CMSI* [25].

The channeled spectrum I^{vacuum} is measured 10 times with the empty cuvette for the position of the mirror M_s, z_v = 20.1 mm. Once the cuvette is filled with water, the corresponding channeled spectrum I^{sample} is recorded 10 times by adjusting the mirror M_s so that its main spectral modulation is identical to that obtained for I^{vacuum} (coefficient β = 0). The position of M_s associated to I^{sample} is then z_s = 16.68 mm.

The difference between the instantaneous phases $\Delta\phi$ of the two spectra is calculated from Eq. (14) and is fitted by a quadratic fit centered at ω_c (Fig. 8), which leads to n_g = 1.3416 +/– 0.0001 and *GVD* = (16.8 +/– 0.7) fs^2/mm, according to Eq. (12) and (13). Here again, the experimental results are in good agreement with the theoretical values. The difference between experimental and theoretical values on n_g can also be explained as being due to the limited accuracy of the sample thickness measurement. For instance, if a 10.013 mm long cuvette was considered, then we would obtain a value identical to the theoretical value of n_g.

In Fig. 8 a drop in the spectral phase value can be noticed at 2.14 rad.fs^{-1}, *i.e.* at the center of the spectral range seen by our spectrometer. This is a consequence of the fact that the light source employed here is actually a combination of two super luminescent emitting diodes, where the overall spectrum is not flat but drops at the center, which leads to a lower spectrometer fringe visibility. Thus, fringe visibility, as well as data acquisition noise such as camera noise and laser source noise can limit the sensitivity in measuring weak *GDD* values.

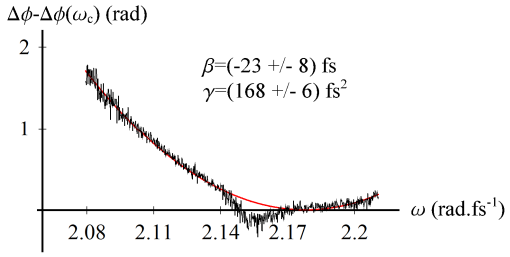

Fig. 8. Δϕ is displayed in black curve between 2.08 and 2.2 rad.fs^{-1}. The red curve corresponds to the fit of Δϕ.

Figure 9(a) shows the relative error of *GVD* according to the position of M_s and it is minimal on a line corresponding to β≈0, as shown in Fig. 9(b) and Fig. 9(c).

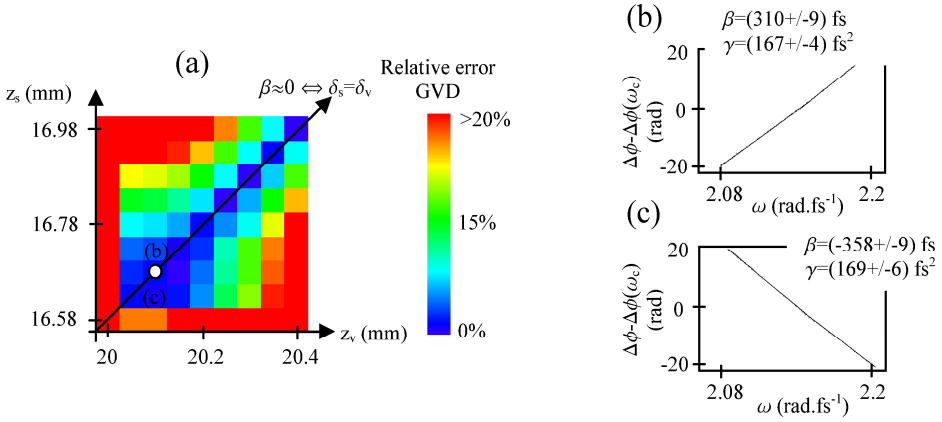

Fig. 9. (a) Relative error of *GVD* according to the position of the mirror M_s with and without water. The white circle corresponds to the specific configuration z_v = 20.1 mm and z_s = 16.68 mm used in the beginning of Section 4.2. (b) Δϕ-Δϕ(ωc) for the configuration z_v = 20.1 mm and z_s = 16.63 mm. (c) Δϕ-Δϕ(ωc) for the configuration z_v = 20.1 mm and z_s = 16.68 mm.

For β = 0, *i.e.* when $\delta_s = \delta_v$, *GVD* and n_g values, (as shown in Fig. 10(a) and in Fig. 10(b) respectively), are stable and agree with the theoretical values, apart from an error in n_g that is assumed to be due to an incorrect value of 10 mm of the cuvette thickness.

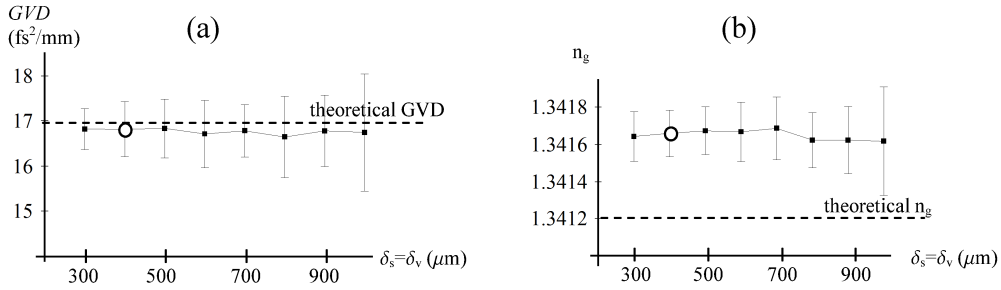

Fig. 10. (a) Measurement of *GVD* for water according to the position of the mirror M_s in the case $\delta_s = \delta_v$. The white circle corresponds to the specific configuration z_v = 20.1 mm and z_s = 16.68 mm used in the beginning of Section 4.2. (b) Measurement of n_g according to the position of the mirror M_s in the case $\delta_s = \delta_v$. The thickness of the cuvette is assumed to be equal to 10 mm for the calculation of *GVD* and n_g.

5. Conclusion

For the first time, processing of phase delivered by the newly introduced *CMSI* method is presented. Progress from the original Master Slave method to Complex Master Slave allowed conservation of phase in the signal captured, by employing complex instead of real masks. This opens several avenues for *CMSI*, one of them being detailed here, employed in dispersion evaluation. In summary, here we propose to use *CMSI* as a new approach to measure *GVD* and group index. Only two channeled spectra, with and without the sample placed in one of the arms of the interferometer have to be measured in order to retrieve the relative phase, followed by a quadratic polynomial fit whose first and second orders are related to group index and *GVD* respectively. In comparison with other methods, there is no need to linearize the data. Not needing linearization speeds up data delivery and reduces the sources of errors.

In addition, compensation of dispersion bias is automatic. The robustness of this technique has been demonstrated on several sets of channeled spectra. It is shown that the most robust results are obtained when the channeled spectrum measured with the sample is adjusted to display a similar modulation to the channeled spectrum without the sample, adjustment that makes the linear coefficient β equal to zero in the relative phase. A maximum deviation of 0.03% from the expected values was measured for the group index n_g, and 1% for the *GVD*. These measurements could be improved by increasing the accuracy of the sample thickness measurement or by accumulating more phase within thicker samples. Another alternative could be to extend the spectral bandwidth within which the phase is measured [17]. A 70 nm bandwidth spectrum was used in the paper but the method is applicable to any bandwidth, including ultra wide bandwidths available by using supercontinuum sources and considering higher-order terms for the fit of the spectral phase.

The measurements were made in transmission, however using a strong reflector in the sample similar measurements can be implemented in reflection. This may open the avenue of a future study on comparing the efficiency of our method with that based on the degradation of the point spread function from the speckle pattern [26].

Finally, our method, with more refinements and adaptations [27], could be used in OCT as an alternative to other methods based on the spectral phase, such as no-dye angiography based on phase methods or polarization sensitive OCT methods. These potential directions of applications should similarly, as shown in this study, take advantage of the CMS method: (i) No need for data resampling; (ii) No need for dispersion compensation. In addition, the CMS provides direct provision of information from multiple depths in the sample (when using a FT, data from outside depths of interest is discarded).

Funding

H2020 Marie Skłodowska-Curie Actions (MSCA) (625509), Engineering and Physical Sciences Research Council (EPSRC) (EP/N019229/1), Innovationsfonden (4107-00011A), H2020 European Research Council (ERC) (754695), National Institute for Health Research Biomedical Research Centre at Moorfields Eye Hospital NHS Foundation Trust (NIHR), the UCL Institute of Ophthalmology, University College London, the Royal Society Wolfson research merit award and Erasmus+.